IMAV2017-13
http://www.imavs.org/pdf/imav.2017.13

Controller Tuning Strategy for Quadrotor MAV Carrying a Cable-suspended Load

Nestor A. Santos Ortiz[*], Edouard Laroche[†], Renaud Kiefer[‡] and Sylvain Durand[§]
ICube UMR 7357, 300 bd. Sébastien Brant - CS 10413 - F-67412 Illkirch Cedex, France

ABSTRACT

This paper presents a controller tuning strategy for a quadrotor MAV carrying a cable-suspended load. In our study, no measurement nor estimation of the load's position is used in the control strategy and only the quadrotor attitude and position are controlled. The tuning of the controllers has been done in order to satisfy mixed H_∞ requirements and a pole-location requirement. The resolution is made with an available tool based on non-smooth optimization. The proposed methodology, allowing to find a good trade-off between fast displacements of the MAV and well damped oscillations of the load, is validated in simulation.

Keywords : PID control, quadrotor, suspended load perturbations, fixed-structure controller tuning.

1 INTRODUCTION

Multirotor micro air vehicles (MAV) are now considered for multiple kinds of missions such as search and rescue [1], surveillance [2], exploration, field recognition and cargo transportation [3]. This project focuses on the payload transport missions, specifically on the problem of carrying a load suspended with a cable. Over the last few years, the increasing demand of this capability on quadrotors has motivated researchers to study this problem and diverse efforts have already been done to solve it. Different control techniques have been already implemented for quadrotor applications with the aim to improve their performances and capabilities.

In general, pioneers on the subject started with the design of the control strategies of quadrotors. Altug *et al.* [4] proposed the use of backstepping controllers for position control considering the dependency with the attitude control. Hamel *et al.* [5] developed control Lyapunov functions by separating the rigid body dynamics and the motors dynamics. They also introduced the use of quaternions for attitude error estimation. Pounds *et al.* presented the design of a controller based on two cascaded loops integrating a double lead compensator and a pure proportional feedback loop [6].

[*]Email address: nestor-alonso.santos-ortiz@insa-strasbourg.fr
[†]Email address: laroche@unistra.fr
[‡]Email address: renaud.kiefer@insa-strasbourg.fr
[§]Email address: sylvain.durand@insa-strasbourg.fr

Returning to the specific problem here discussed, it can be viewed and analyzed from different angles. One approach focuses on the control of the suspended load so it follows a specific trajectory while damping the oscillations. Faust *et al.* developed an algorithm based on machine learning for the generation of trajectories reducing the swing of the load [7]. They, as most of other researchers, use the model of a rigid 3D pendulum for the cable-suspended load. Dai *et al.* preferred to use a more accurate model considering the cable as a series of connected links and they design a controller implementation to align these links vertically while transporting the load to a desired position [8]. In their results, an adaptive controller is used to compensate the payload's mass uncertainty that demonstrates better performances than a PID controller with constant gains. Other design methods have been proposed in order to reject the perturbations generated by the oscillations of the suspended load seen as a disturbance. For example, in [9, 10], nonlinear controllers are presented for trajectory tracking based on partial feedback linearization and on the backstepping technique, respectively. In [11], both disturbance rejection and swing reduction problems are considered. A nonlinear H_∞ controller added to a control law obtained by the Lyapunov redesign technique is proposed and evaluated in simulation. Finally, a third variant of the problem considers the case of a load carried by multiple cooperative MAVs [12].

In most of the cases, it is considered that the complete state vector is measurable. For this reason, experimentation is frequently done in rooms equipped with motion capture vision systems. A problem that arises here is the implementation of these control strategies for outdoor flights. In this paper, the classical PID control strategy is implemented on a quadrotor where no sensor is employed to estimate the orientation of the cable nor the load's position. The PID structure here implemented is similar to the B-type presented in [13] by Szafranski where derivation is applied directly on the measurement signal and not on the error signal. The PID controller has been commonly used on MAVs and, as in many other applications, it is frequently included in studies where different controllers are to be evaluated [14]. Moreover, this kind of controller is commonly implemented in open source and commercial autopilot frameworks used for MAV. The analysis of the controller performance is presented with a tuning strategy for the gain parameters with optimization algorithms considering the dynamic model of the load in the system.

In Section 2, the complete system modeling is detailed. Section 3 details the attitude control strategy, including simulations results. Section 4 presents an analysis for the position control. Section 6 concludes the paper and discusses some future work.

2 System Modeling

After introducing the quadrotor MAV structure used for the present study, the modeling of the system with the suspended load is presented using the Euler-Lagrange formalism. The suspended load is considered as a pendulum with the cable assumed to be a rigid massless link attached at a certain distance under the center of gravity of the quadrotor.

2.1 *Millenium quadrotor*

The *Millenium* quadrotor, developed at INSA Strasbourg, is considered in this project [15]. Its structure is entirely made with composite materials that offer excellent mechanical properties while minimizing the weight, increasing the payload that it can carry up-to 1 kg. Its configuration is of X type, however its structure has only a longitudinal symmetry. The two frontal arms are more open so they do not appear in the field of view of a camera looking towards that direction, see Figure 1.

A Pixhawk Autopilot board is used for the control of this drone which runs the PX4 firmware pilot. PID type controllers are used by default and their parameters can be easily modified via a ground control station.

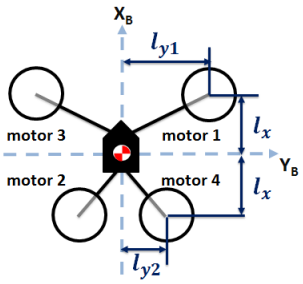

Figure 1: INSA's quadrotor's framework and motors map.

2.2 *Kinematics and system coordinates*

Two main reference frames are used for modeling the MAV: the inertial frame attached to a point in the earth ($\mathscr{R}_E = \boldsymbol{X_E}, \boldsymbol{Y_E}, \boldsymbol{Z_E}$) and the body fixed frame ($\mathscr{R}_B = \boldsymbol{X_B}, \boldsymbol{Y_B}, \boldsymbol{Z_B}$). Inertial frame is defined as NED type since it is the case in the PX4 board controller.

Position vector $\boldsymbol{\xi} \in \mathscr{R}_E$ is defined as the position of the body frame origin in the inertial frame coordinate system.

$$\boldsymbol{\xi} = \begin{bmatrix} x_E & y_E & z_E \end{bmatrix}^T \tag{1}$$

Euler angles are used to define the attitude of the quadrotor with respect to the inertial frame in the following order: yaw (ψ) around the Z-axis, then pitch (θ) around Y-axis and finally roll (φ) around the X-axis.

$$\boldsymbol{\eta} = \begin{bmatrix} \varphi & \theta & \psi \end{bmatrix}^T \tag{2}$$

The rotation matrix $\boldsymbol{R_E^B}$ from body to inertial frame is defined in (3).

$$\boldsymbol{R_B^E} = \begin{bmatrix} c_\psi c_\theta & c_\psi s_\theta s_\varphi - s_\psi c_\varphi & c_\psi s_\theta c_\varphi + s_\psi s_\varphi \\ s_\psi c_\theta & s_\psi s_\theta s_\varphi + c_\psi c_\varphi & s_\psi s_\theta c_\varphi - c_\psi s_\varphi \\ -s_\theta & c_\theta s_\varphi & c_\theta c_\varphi \end{bmatrix} \tag{3}$$

To transform the derivatives of the Euler angles from the inertial frame, $\dot{\boldsymbol{\eta}}$, to the body frame, $\boldsymbol{\omega_B}$, the transformation matrix $\boldsymbol{J}$ defined in Equation (4) is used.

$$\boldsymbol{\omega_B} = \begin{bmatrix} p \\ q \\ r \end{bmatrix} = \boldsymbol{J} \cdot \dot{\boldsymbol{\eta}} = \begin{bmatrix} 1 & 0 & -s_\theta \\ 0 & c_\varphi & s_\varphi c_\theta \\ 0 & -s_\varphi & c_\varphi c_\theta \end{bmatrix} \begin{bmatrix} \dot{\varphi} \\ \dot{\theta} \\ \dot{\psi} \end{bmatrix} \tag{4}$$

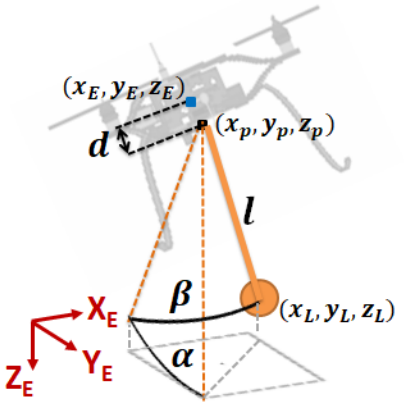

Figure 2: Suspended load parametrization.

For the load displacement analysis, a new coordinate frame fixed to the pendulum ($\mathscr{R}_P = \boldsymbol{X_P}, \boldsymbol{Y_P}, \boldsymbol{Z_P}$) is defined with its origin on the attachment point and with $\boldsymbol{Z_P}$ coincident with the cable. The rotation matrix $\boldsymbol{R_P^E}$ from the pendulum frame to the inertial frame is defined with angles α and β corresponding to rotation of the pendulum firstly around the $\boldsymbol{X_E}$ axis and then around the already rotated $\boldsymbol{Y_E'}$ axis, as illustrated in Figure 2.

$$\boldsymbol{R_P^E} = \begin{bmatrix} c_\beta & 0 & s_\beta \\ s_\alpha s_\beta & c_\alpha & -s_\alpha c_\beta \\ -c_\alpha s_\beta & s_\alpha & c_\alpha c_\beta \end{bmatrix} \tag{5}$$

In addition, the position of the cable fixation point is under a distance d from the center of gravity of the quadrotor which is chosen as the body frame origin. Finally, the position vector of the load in the inertial frame, $\boldsymbol{\xi_L}$, is obtained in Equation (6) with l the length of the cable.

$$\boldsymbol{\xi_L} = \begin{bmatrix} x_L \\ y_L \\ z_L \end{bmatrix} = \boldsymbol{\xi} + \boldsymbol{R_B^E} \begin{bmatrix} 0 \\ 0 \\ d \end{bmatrix} + \boldsymbol{R_L^E} \begin{bmatrix} 0 \\ 0 \\ l \end{bmatrix} \tag{6}$$

2.3 Forces and torques

The quadcopter is an under-actuated system since only four propellers induce the movement while it has a total of 6 degrees of freedom. In Figure 3, the forces and moments induced by the propellers are illustrated. They are considered to be proportional to the square of the propeller rotation speed:

$$\begin{cases} F_i = k_f \cdot \omega_i^2 \\ \tau_i = k_c \cdot \omega_i^2 \end{cases} \tag{7}$$

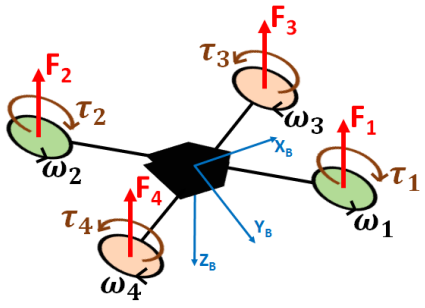

Figure 3: Forces and moments induced by the propellers.

To simplify the analysis, a change among the input variables is defined as following: the control inputs are defined as the total thrust, T, and the torques, τ_φ, τ_θ and τ_ψ, with respect to the three body frame axis. These new inputs variables depend on the rotation speed of propellers, ω_i, and are calculated with Equation (8). The matrix used in this equation is defined considering the particular structure geometry of the quadrotor of this study depicted in Figure 1:

$$\begin{bmatrix} T \\ \tau_\varphi \\ \tau_\theta \\ \tau_\psi \end{bmatrix} = \begin{bmatrix} k_f & k_f & k_f & k_f \\ -k_f l_{y1} & k_f l_{y2} & k_f l_{y1} & -k_f l_{y2} \\ k_f l_x & -k_f l_x & k_f l_x & -k_f l_x \\ k_c & k_c & -k_c & -k_c \end{bmatrix} \begin{bmatrix} \omega_1^2 \\ \omega_2^2 \\ \omega_3^2 \\ \omega_4^2 \end{bmatrix} \tag{8}$$

2.4 Dynamic model

Euler-Lagrange equations are used to obtain the dynamic model of the complete system : quadrotor with suspended load. The translational kinetic energy is composed by both the quadrotor and the load energies :

$$K_{translation} = \frac{1}{2}\left(m\dot{\boldsymbol{\xi}}^T\dot{\boldsymbol{\xi}} + m_L\dot{\boldsymbol{\xi}_L}^T\dot{\boldsymbol{\xi}_L}\right) \tag{9}$$

where m is the quadrotor's mass and m_L is the load's mass. On the other hand, considering the load as a punctual mass, its rotational kinetic energy is neglected and only the quadrotor energy is included :

$$K_{rotation} = \frac{1}{2}\boldsymbol{\omega_B}^T\boldsymbol{I}\boldsymbol{\omega_B} \tag{10}$$

where I is the inertial matrix of the quadrotor with respect to the body frame and which is considered as a diagonal one ($I = \mathrm{diag}(I_{xx}, I_{yy}, I_{zz})$) since the MAV principal axes are supposed to be coincident with the body frame axes for simplification. However, in reality they are slightly rotated.

Finally, the potential energy is defined in Equation (11) where g represents the gravity constant. The negative sign of this equation is due to the positive direction of the Z axis which is downwards.

$$U = -m_D g\boldsymbol{Z_E}^T\boldsymbol{\xi} - m_L g\boldsymbol{Z_E}^T\boldsymbol{\xi_L} \tag{11}$$

The dynamic of the system is summarized with the Lagrangian L equal to the kinetic energy minus the potential energy.

$$L = K_{translation} + K_{rotation} - U \tag{12}$$

Then, the Euler-Lagrange equations represents the equations of motion of the system for the generalized coordinates $\boldsymbol{q} = \begin{bmatrix} x_E & y_E & z_E & \varphi & \theta & \psi & \alpha & \beta \end{bmatrix}^T$:

$$\frac{d}{dt}\left[\frac{\partial L}{\partial \dot{q}_i}\right] - \frac{\partial L}{\partial q_i} = Q_i, \quad i = 1, ..., 8 \tag{13}$$

The generalized force vector $\boldsymbol{Q}$ is defined by the input force $\boldsymbol{F}$, the input torque $\boldsymbol{\tau}$ and the gyroscopic effect moment of the rotors $\boldsymbol{\Gamma}$. Note that the frictional forces due to air resistance have been neglected.

$$\boldsymbol{Q} = \begin{bmatrix} \boldsymbol{F} \\ \boldsymbol{\tau} - \boldsymbol{\Gamma} \\ \boldsymbol{0_{2\times 1}} \end{bmatrix} \tag{14}$$

$$\boldsymbol{F} = \boldsymbol{R_B^E}\begin{bmatrix} 0 & 0 & -T \end{bmatrix}^T \tag{15}$$

$$\boldsymbol{\tau} = \begin{bmatrix} \tau_\varphi & \tau_\theta & \tau_\psi \end{bmatrix}^T \tag{16}$$

The gyroscopic moments of the rotors are calculated using Equation (17) with $\Omega = \omega_1 + \omega_2 - \omega_3 - \omega_4$ and I_r correspond to the angular moment of rotors.

$$\boldsymbol{\Gamma} = I_r\left(\boldsymbol{\omega_B} \times \boldsymbol{Z_B}\right)\Omega = I_r \begin{bmatrix} p \\ q \\ r \end{bmatrix} \times \begin{bmatrix} 0 \\ 0 \\ 1 \end{bmatrix} \Omega = \begin{bmatrix} I_r q\Omega \\ -I_r p\Omega \\ 0 \end{bmatrix} \tag{17}$$

Finally using the matrix representation of the Euler-Lagrange equations, motion equation can be written as follows.

$$\boldsymbol{M(q)\ddot{q}} + \boldsymbol{C(q,\dot{q})\dot{q}} + \boldsymbol{G(q)} = \boldsymbol{Q} \tag{18}$$

$$\boldsymbol{\ddot{q}} = \boldsymbol{M(q)}^{-1}\left(\boldsymbol{Q} - \boldsymbol{C(q,\dot{q})\dot{q}} - \boldsymbol{G(q)}\right) \tag{19}$$

Matrices $\boldsymbol{M(q)}$, $\boldsymbol{C(q,\dot{q})}$ and $\boldsymbol{G(q)}$ have been easily obtained with a Matlab script but they are very extensive to appear in this paper.

2.5 *Propellers dynamic model identification*

Dynamic model of the motor-propeller set is commonly identified by a first-order model [16], with a time constant τ and a gain K in addition to a delay d due to the period of the pulse-width modulated input signal to the motors ESC.

$$T(s) = e^{-d \cdot s} \frac{K}{1 + \tau \cdot s} \tag{20}$$

Identification experimental data showed that the time constant is different when the motor speed is increased and when it is lowered. In addition, the static gain identified follows a quadratic behavior in function of the positive pulse duration of the PWM input of ESC controllers which varies from 1.1 ms to 1.9 ms with a frequency of 400Hz. Then, the non linear model in Equation (21) has been defined, with y the rotation speed in RPM and u the ESC input in ms.

$$\begin{aligned} &K = a_2 u^2 + a_1 u + a_0 \\ &\begin{cases} \dot{y} = \frac{1}{\tau_1}(Ku - y) & , Ku - y \geq 0 \\ \dot{y} = \frac{1}{\tau_2}(Ku - y) & , Ku - y < 0 \end{cases} \end{aligned} \tag{21}$$

A noticeable improvement fit has been observed with the proposed nonlinear model compared to the linear model.

2.6 *System parameters*

The dimensions and mass parameters of the quadrotor have been directly measured. Furthermore, the diagonal inertia matrix values have been estimated with the compound pendulum method described in [17]. The identified parameter values are presented in Table 1 and compared to the values obtained with the CAD model of the system. As observed, the CAD model values help as an approximation to validate the coherency of the measurements.

Table 1: Dimensions, mass and inertia parameters.

DATA	CAD	Measurements
m $[kg]$	2.834	2.832 ± 0.02
l_x $[m]$	0.262	0.270 ± 0.005
l_{y1} $[m]$	0.284	0.295 ± 0.005
l_{y2} $[m]$	0.222	0.225 ± 0.005
I_{xx} $[kg \cdot m^2]$	0.064	[0.054 - 0.061]
I_{yy} $[kg \cdot m^2]$	0.077	[0.060 - 0.068]
I_{zz} $[kg \cdot m^2]$	0.127	[0.107 - 0.118]

Thrust coefficient has been approximated from experimental flight data where the quadrotor stayed on a hover position. Drag coefficient has not been identified and an approximated value has been chosen based on online databases.

3 Attitude Control

As already mentioned before, the interest of this paper is not to design a better controller structure for this application, but to suggest an original strategy to calculate the best parameters of the imposed controllers which structure is defined in Figure 4. It is a pure proportional controller in the outer-loop cascaded with a PID in the inner-loop.

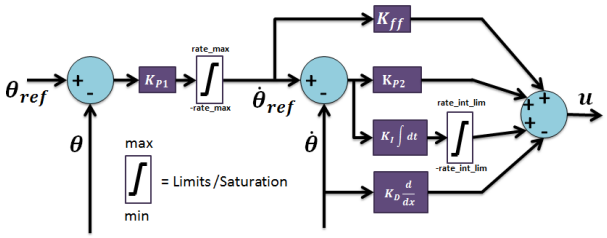

Figure 4: PX4 attitude PID controller structure.

3.1 *Tuning of the control parameters*

For the tuning of the controller parameters, a solution with optimization algorithms for non-smooth and non-convex problems is available (see [18, 19]). The optimization problem solved by this algorithm, considering only one plant model, is of the form

$$\begin{aligned} &\underset{p \in \Re}{\text{minimize}} \ \max_{i=1,\ldots,n_f} \{f_i(p)\} \\ &\text{subject to} \ \max_{j=1,\ldots,n_g} \{g_j(p)\} \leq 1 \end{aligned} \tag{22}$$

where p is the vector of tunable parameters. Functions f_i and g_j represent the requirements, considered as soft and hard respectively. There can be as many requirements as desired in the form of H_2 or H_∞ norms of weighted transfer functions, or in terms of a pole location constrain. Values γ_s and γ_h represent the optimization results for the soft and hard requirements.

Moreover, this tuning method can be easily implemented in Matlab with the *'systune'* tool. Here, this has been used looking to satisfy three different hard performance requirements (same results are obtained with only soft requirements):

Req 1: Maximum tracking error from the angle reference to the angle measurement in the frequency domain;

Req 2: Maximum gain from disturbance to angle measurement in the frequency domain;

Req 3: Pole location of the closed-loop system.

To simplify the problem, the dynamic model for each of the controlled variables has been separated and simplified. Two different models have been used for roll and pitch, the

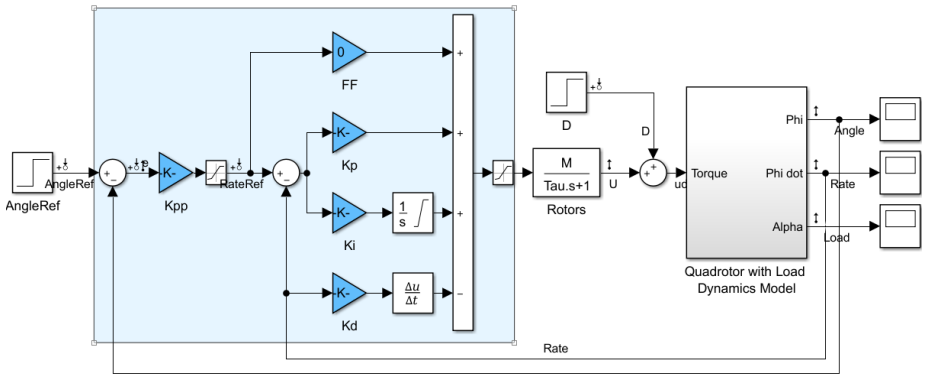

Figure 5: Simplified control system for roll (*KA2*).

first one without considering the pendulum load, and the second one including it. This way two different sets of parameters for attitude controllers have been obtained and evaluated. The following notations are used for next references:

***KA1*:** Tuning of the parameters when considering the model of the system without the load;

***KA2*:** Tuning of the parameters when considering the model of the system with the load.

Figure 5 shows the general aspect of the simulink model used for tuning the roll controller in case *KA2*. A linear model has been used for the actuators with a gain M from the control output to the system input due to the PX4 normalized mixer (mixer transforms the controller outputs into the motors ESC control inputs).

For both cases, the weighting functions used on the performance channel have been adjusted iteratively by looking for the most demanding performances that could be satisfied ($\gamma_h \leq 1$). In a first step, the bandwidth, the reject of perturbation, the damping ratio and the decay ratio (associated to the phase and the real part of the dominant poles respectively) of dominant poles were required to a relative high value for this specific application. The system could never satisfy these constrains but this gave an intuition of the performances limits of the system. In a next step, the requirements have been lowered until all of them could be satisfied. Figures 6(a) and 6(b) show the evaluation of the final requirements for cases *KA1* and *KA2* respectively.

It can be observed that in the case of *KA1*, the bandwidth of the system is a little higher than in the case of *KA2*. Note that when a higher bandwidth was requested in the case of *KA2*, it could not be satisfied without affecting the stability of the system (reducing the damping ratio and decay component for the pole location constrain).

3.2 Simulation results

To evaluate roll and pitch controllers, two different tests have been performed in simulation.

In the first test, the MAV is controlled to be on the hover state, and the load is initially perturbed. Specifically, the load is initialized with angles α and β of $20°$. Figure 7 shows the results for the control of roll attitude, for both set of controller parameters *KA1* and *KA2*. The response for pitch is almost the same as the obtained for roll. As it can be clearly observed, with the *KA2* parameters, the load oscillations are rapidly attenuated, contrarily to the case with parameters *KA1*.

In a second test, the MAV attitude angles ϕ and θ were initially set to $20°$, and the control reference is the horizontal attitude. This time the load is initially at rest but it will be excited by the horizontal movement induced with the initial attitude of the MAV. For this test, results are presented in Figure 8. Again, with the controllers *KA2*, the oscillations of the load are more rapidly attenuated while the reference attitude is also reached.

These results already demonstrate that good stability performances can be achieved considering the model of the load in the tuning process, even when no feedback of the load position is used in the control strategy.

4 POSITION CONTROL

The same controller structure as used for attitude in section 3 is employed for the position control. Note that for horizontal movements, the position controller is cascaded with attitude controller. The X, Y and Z control signals define a reference thrust vector in the inertial frame which orientation is used to define the pitch and roll reference angles. Besides, in function of the current attitude of the drone, the thrust vector is redefined and its magnitude is calculated for the control of the altitude. As a result, control is done for X, Y, Z, and yaw. Again, the same process followed for the attitude controllers tuning has been implemented in this case. Two models have been also used :

***KP1*:** Tuning of the parameters when considering the model of the system without the load and *KA1* attitude controllers;

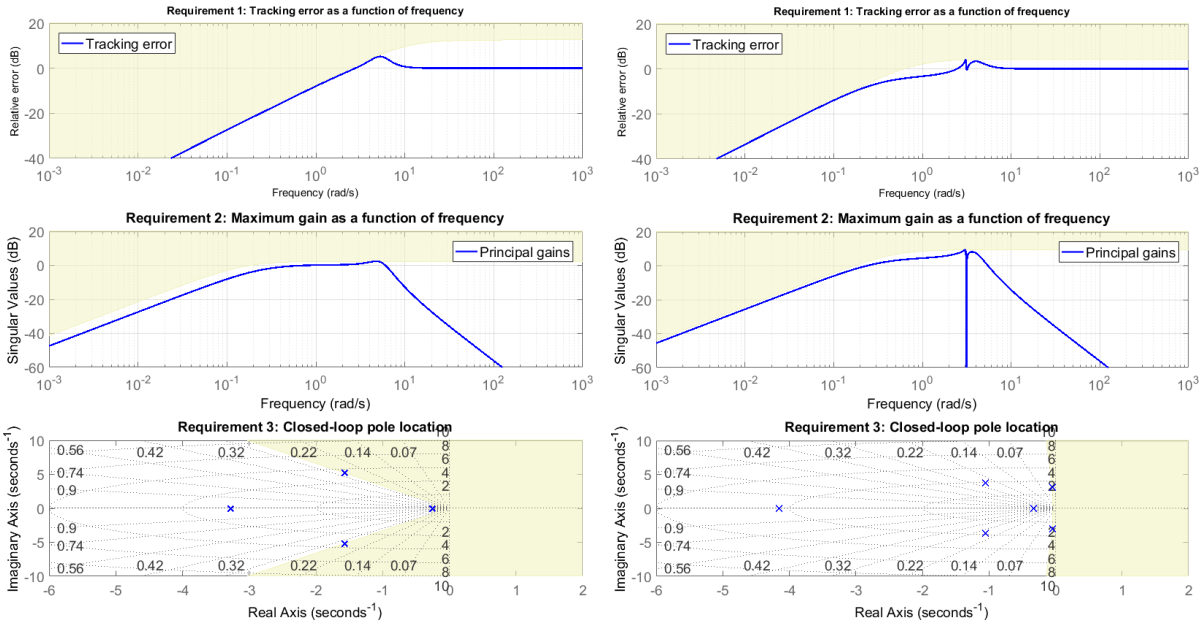

(a) KA1. (b) KA2.

Figure 6: Requirements for roll controller tuning.

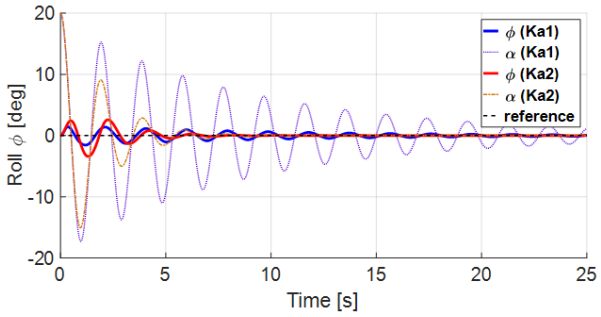

Figure 7: Quadrotor's roll attitude in time, first test.

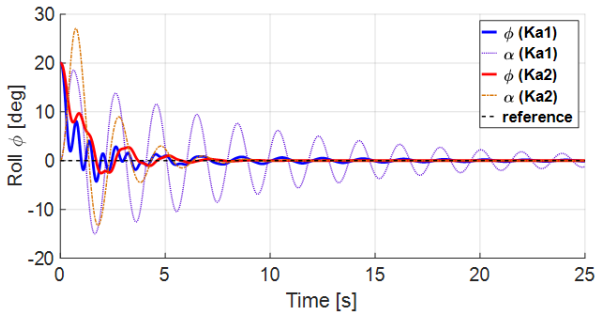

Figure 8: Quadrotor's roll attitude in time, second test.

trollers.

This time, only one test has been used for evaluation. From an initial position at rest, the test consisted in step variations of the reference signal. Note that, rather than using a trajectory generation algorithm as it is usually the case, steps have been used to fully excite the system and emphasize its stability properties. The reference positions formed a square trajectory with the center in the initial position. A 3D visualization of thethis test appears on Figure 9.

The comparison of the reference tracking results with the different sets of parameters can be appreciated in Figure 10. On the one hand, with parameters *KP1-KA1*, Figure 10(a), the system shows relative good performances. The reference is rapidly reached with a small overshot and few oscillations. On the other hand, with parameters *KP2-KA2*, Figure 10(b), the system is less dynamic. However, in terms of the stabilization of the load, better results are obtained with the later parameters. As it can be observed in Figure 11, with the second set of controller parameters, the oscillations of the load are more attenuated and the highest amplitude is around four times lower.

5 Discussion on the Tuning Strategy

From our experience in the tunning process, we draw several recommendations.

***KP2*:** Tuning of the parameters when considering the model of the system with the load and *KA2* attitude con-

Model with or without the load. It is possible to use a synthesis model that does not include the load, which simplifies

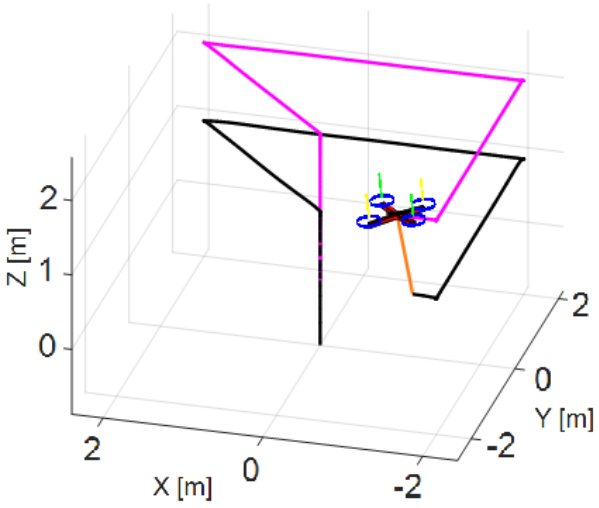

Figure 9: 3D visualization of the position control simulation (with controller *KP2* and *KA2*)

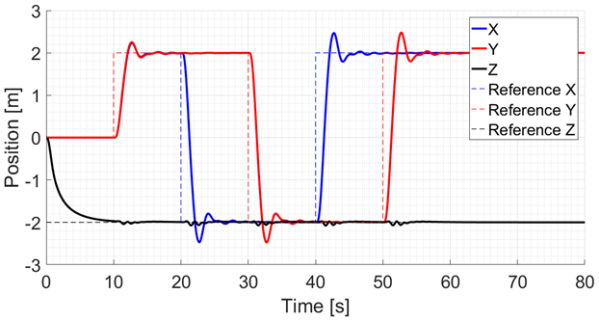

(a) Controller *KP1* and *KA1*.

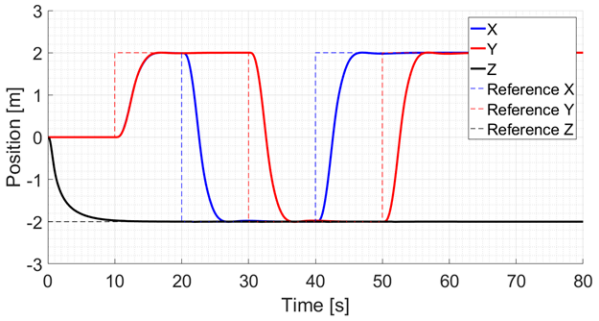

(b) Controller *KP2* and *KA2*.

Figure 10: Quadrotor's position with respect to time.

the modeling step. With this model, it is possible to obtain a much faster control of the orientation and the position of the UAV, but at the cost of undamped or unstable load oscillations if the bandwidth is chosen higher than the load oscillation frequency. The model including the load displacements was found convenient to tune a controller that damps the load oscillations.

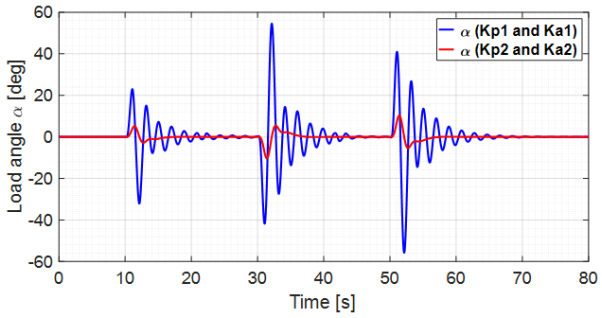

(a) Angle α.

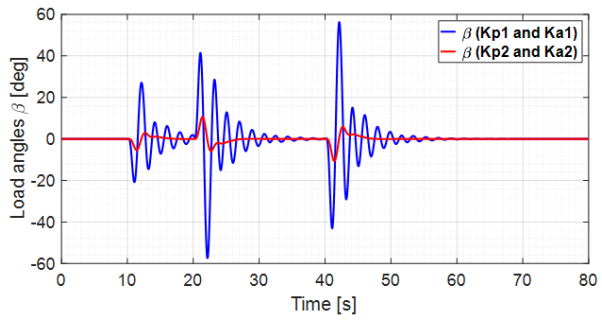

(b) Angle β.

Figure 11: Load angle α and β during the position control test.

Pole location requirement only. In an attempt to simplify the requirements specification, the pole location constrain has been used as the only requirement. However, we observed that the resulting dynamics of the UAV is degraded and then sticks to the dynamics of the load.

Remove the pole location requirement. We replaced the pole location by a frequency requirement on the transfer between the reference and the load displacement, which results in purely frequency-domain requirements. Even if these requirements allowed to damp the load oscillations, we obtained a better results by including the pole placement requirements. Notice that once the pole placement requirement is included, the requirements on the transfer between the reference and the load displacement can be removed without any drawback.

Hard vs soft requirements. The possibility of prioritizing some of the requirements (using hard and soft requirements) has also been investigated. However, better results have been obtained by keeping the same strength for all requirements.

6 Conclusions and Future Work

The problem of the control of a quadrotor MAV with a cable-suspended load has been studied. The modeling of the system including the load has been described. It has been

considered that the attachment point of the cable is not coincident with the center of gravity of the MAV, allowing the load to induce perturbations on the drone's attitude. Moreover, a tuning methodology for the controllers has been proposed in order to find a good trade-off between the response time of the vehicle and the damping of the load oscillations, even when there is no feedback of them. The validity of this methodology has been proved with simulations. This can be useful during outdoor flights with standard quadrotors, avoiding the need of adding sensors for the load position estimation and maintaining the simplicity of this type of control implementation. In future work, the evaluation of the tuned controllers will be performed experimentally using the *Millenium* quadrotor from INSA Strasbourg to observe the robustness against non modeled dynamics and uncertainty on the identified parameters of the system.

ACKNOWLEDGEMENTS

This project is supported by the *CoreDrone* project, an internal project from ICube Laboratory, and INSA Strasbourg.

REFERENCES

[1] T. Tomic, K. Schmid, P. Lutz, A. Domel, M. Kassecker, E. Mair, I. L. Grixa, F. Ruess, M. Suppa, and D. Burschka. Toward a fully autonomous UAV: Research platform for indoor and outdoor urban search and rescue. *IEEE Robotics & automation magazine*, 19(3):46–56, 2012.

[2] H. C. Yang, R. AbouSleiman, B. Sababha, E. Gjioni, D. Korff, and O. Rawashdeh. Implementation of an autonomous surveillance quadrotor system. In *AIAA Infotech Aerospace Conference*, page 2047, 2009.

[3] R. Mileham. Prime movers. *Engineering & Technology*, 11(4):70–72, 2016.

[4] E. Altug, J. P. Ostrowski, and R. Mahony. Control of a quadrotor helicopter using visual feedback. In *IEEE Int. Conf. Robotics and Automation*, pages 72–77 vol.1, 2002.

[5] T. Hamel, R. Mahony, R. Lozano, and J. Ostrowski. Dynamic modelling and configuration stabilization for an x4-flyer. *IFAC Proceedings Volumes*, 35(1):217–222, 2002.

[6] P. Pounds, R. Mahony, P. Hynes, and J. M. Roberts. Design of a four-rotor aerial robot. In *Australasian Conference on Robotics and Automation (ACRA)*, pages 145–150. Australian Robotics & Automation Association, 2002.

[7] A. Faust, I. Palunko, P. Cruz, R. Fierro, and L. Tapia. Learning swing-free trajectories for uavs with a suspended load. In *IEEE Int. Conf. Robotics and Automation*, pages 4902–4909, May 2013.

[8] S. Dai, T. Lee, and D. S. Bernstein. Adaptive control of a quadrotor UAV transporting a cable-suspended load with unknown mass. In *IEEE Conf. Decision and Control*, pages 6149–6154, December 2014.

[9] I. H. Beloti Pizetta, A. S. Brando, and M. Sarcinelli-Filho. Modelling and control of a quadrotor carrying a suspended load. In *Education and Development of Unmanned Aerial Systems (RED-UAS) 2015 Workshop Research*, pages 249–257, November 2015.

[10] K. Klausen, T. I. Fossen, and T. A. Johansen. Nonlinear control of a multirotor UAV with suspended load. In *Int. Conf. Unmanned Aircraft Systems (ICUAS)*, pages 176–184, June 2015.

[11] Guilherme V Raffo and Marcelino M de Almeida. Nonlinear robust control of a quadrotor uav for load transportation with swing improvement. In *American Control Conference (ACC), 2016*, pages 3156–3162. IEEE, 2016.

[12] K. Sreenath and V. Kumar. Dynamics, control and planning for cooperative manipulation of payloads suspended by cables from multiple quadrotor robots. June 2013.

[13] G. Szafranski and R. Czyba. Different approaches of pid control uav type quadrotor. *International Micro Air Vehicles (IMAV)*, 2011.

[14] A. Rodic, G. Mester, and I. Stojkovic. Qualitative evaluation of flight controller performances for autonomous quadrotors. In *Intelligent Systems: Models and Applications*. Springer, January 2013.

[15] R. Kiefer and M. Vedrines. Proposition of design method and optimization of multirotors composite structures. In *International Micro Air Vehicles (IMAV)*, Aachen, Germany, September 2015.

[16] E. Roussel, V. Gassmann, and E. Laroche. Modelling and identification of a coaxial birotor UAV from scarce flight data. In *Proc. European Control Conf. (ECC)*, pages 2158–2164, June 2016.

[17] H. A. Soule and M. P. Miller. The experimental determination of the moments of inertia of airplanes. Technical Report 467, National Advisory Committee for Aeronautics, Langley Field, VA, USA, 1934.

[18] P. Apkarian, P. Gahinet, and C. Buhr. Multi-model, multi-objective tuning of fixed-structure controllers. In *European Control Conference (ECC)*, pages 856–861. IEEE, 2014.

[19] P. Apkarian and D. Noll. Nonsmooth H_∞ synthesis. *IEEE Transactions on Automatic Control*, 51(1):71–86, 2006.